Viscosity of two-dimensional strongly coupled dusty plasma modified by a perpendicular magnetic field

Yan Feng* and Wei Lin
Center for Soft Condensed Matter Physics and Interdisciplinary Research, College of Physics, Optoelectronics and Energy, Soochow University, Suzhou 215006, China

M. S. Murillo
Department of Computational Mathematics, Science and Engineering, Michigan State University, East Lansing, Michigan 48824, USA
(Received 24 August 2017; published 28 November 2017)

Transport properties of two-dimensional (2D) strongly coupled dusty plasmas have been investigated in detail, but never for viscosity with a strong perpendicular magnetic field; here, we examine this scenario using Langevin dynamics simulations of 2D liquids with a binary Yukawa interparticle interaction. The shear viscosity η of 2D liquid dusty plasma is estimated from the simulation data using the Green-Kubo relation, which is the integration of the shear stress autocorrelation function. It is found that, when a perpendicular magnetic field is applied, the shear viscosity of 2D liquid dusty plasma is modified substantially. When the magnetic field is increased, its viscosity increases at low temperatures, while at high temperatures its viscosity diminishes. It is determined that these different variational trends of η arise from the different behaviors of the kinetic and potential parts of the shear stress under external magnetic fields.

DOI: 10.1103/PhysRevE.96.053208

I. INTRODUCTION

Strongly coupled plasma refers to a collection of charged particles where the potential energy between nearest neighbors is higher than the averaged kinetic energy [1]. Due to the strong coupling between charged particles, they cannot move past one another easily, so the strongly coupled plasma has correlations similar to those of liquids or solids [2–5]. In experiments, dusty plasmas are strongly coupled due to the extremely low charge-to-mass ratio of dust particles [6]; pure ion plasmas [7] and ultracold plasmas [8] are strongly coupled due to the extremely low temperature of ions. In astrophysical settings, strongly coupled plasmas also exist, such as in white dwarfs [9] and neutron stars [10], due to the extreme high density of particles.

Most plasmas exist in complicated magnetic fields, such as various fusion plasmas of magnetic confinement tokamaks [11] and stellarators [12], inertial confinement fusion devices (e.g., Omega and NIF facilities [13]), and pinches [14]. One type of star, the magnetar, has extremely powerful magnetic fields [15]. Under these external magnetic fields, the collective behaviors of plasmas are expected to be modified fundamentally [16,17]. Due to their imaging diagnostics and simple simulation methods, dusty plasmas provide an excellent experimental and theoretical platform to study the dynamics of strongly coupled plasmas under magnetic fields.

In the laboratory, dusty plasma can be easily obtained by introducing micron-sized dust particles of solid matter into an ionized gas [2–5,18,19]. In the plasma environment, these dust particles would be charged to a steady state within microseconds, with a typical charge of -10^3e to -10^5e. In experiments, these charged dust particles can be levitated and confined by the electric field in the plasma sheath, so that they can self-organize into a single layer, i.e., forming a two-dimensional (2D) suspension, with negligible out-of-plane motion [20]. Within this single layer, due to the shielding effects of free electrons and ions, the interaction between dust particles can be accurately modeled as the Yukawa, or Debye-Hückel, potential [21,22], with the form $\phi(r) = Q^2\exp(-r/\lambda_D)/4\pi\epsilon_0 r$, where Q is the dust charge and λ_D is the Debye screening length. Due to the strong coupling of these dust particles, the collection of dust particles exhibits behaviors of liquids [23,24] and solids [18,25]. Molecular dynamics (MD) simulations of 2D Yukawa liquids and solids have been widely used to study behaviors of 2D dusty plasmas [16,17,26–37].

As an important transport coefficient arising from the interparticle interactions [20], the shear viscosity of 2D dusty plasmas has been studied intensively for more than a decade [29,31,38]. In dusty plasma studies, the viscosity has been quantified using two methods, with and without a macroscopic shear flow. For the first method, in dusty plasma experiments, laser beams can be used to drive macroscopic shear flows in a dusty plasma crystal, resulting in a flow pattern with temperature nonuniformities and strong shear [38–40]. Then the viscosity can be obtained either by fitting the flow profile to the hydrodynamical Navier-Stokes equation [38,39] or from the viscosity constitutive relation (ratio of the internal shear stress and shear rate), which we later call the hydrodynamic method [40]. In dusty plasma simulations with a sustained macroscopic shear, its viscosity has also been obtained using the constitutive relation [31,32]. For the second method, in the equilibrium simulation of dusty plasmas, i.e., without any macroscopic gradients such as shear, the viscosity has been calculated using the Green-Kubo relation [29]. Later, the Green-Kubo relation was also used with the experimental data, as in [20], to estimate the viscosity value. It was thought that the viscosity results obtained from these two methods do not show substantial variation. In [41] and [42], a more elaborate

*fengyan@suda.edu.cn

laser-manipulation experiment was performed with separate laser beams for heating and shear, and this was again used with the hydrodynamic method to calculate the viscosity. The new result in [42] suggests that the viscosity obtained from the Green-Kubo relation with the dusty plasma experimental data can be 60% higher than the viscosity from the hydrodynamic method. This result of a systematic quantitative difference has not yet been confirmed by other experimenters, but for our purposes it does not matter much, as we are more interested here in trends in the viscosity as the magnetic field is varied than in the exact numerical value of the viscosity.

Recently, magnetized dusty plasmas have attracted a lot of attention, both in experiments and in theory. For 2D dusty plasma systems under magnetic fields, the particle transport of diffusion [16,17] and heat transport [36,37] have already been studied theoretically. However, study of the momentum transport of the shear viscosity for 2D dusty plasmas under external magnetic fields is still lacking, from our literature search.

Here, we study the viscosity of a 2D layer of dust in a plasma with its motion modified by a perpendicular magnetic field. We use Langevin MD simulation data. With the perpendicular magnetic field, the thermal motion of dust particles should be coupled with the gyro motion [17], so that momentum transport behavior is fundamentally modified. The Green-Kubo relation is employed here to estimate the shear viscosity of 2D dusty plasmas from the motion of individual dust particles. We show that, for 2D dusty plasma liquids, the variation of the viscosity as a function of the magnetic field is different: at low temperatures the viscosity rises with the magnetic field, however, at high temperatures the viscosity diminishes with the magnetic field. The underlying interpretations of the different trends are discussed.

II. METHODS

A. Simulation methods

To mimic 2D dusty plasmas, we perform Langevin MD simulations, where the binary interparticle interaction is chosen to be the Yukawa potential. All simulated 1024 particles are constrained within a single 2D plane with the periodic boundary conditions. The equation of motion for each particle is $m\ddot{\mathbf{r}}_i = Q\dot{\mathbf{r}}_i \times \mathbf{B} - \nabla\Sigma\phi_{i,j} - \nu m\dot{\mathbf{r}}_i + \zeta_i(t)$, where $Q\dot{\mathbf{r}}_i \times \mathbf{B}$ is the Lorentz force due to the perpendicular magnetic field, and $-\nabla\Sigma\phi_{i,j}$ represents the interparticle interaction. For the latter terms, $-\nu m\dot{\mathbf{r}}_i$ is the frictional gas drag acting on moving dust particles, while $\zeta_i(t)$ is the random kick due to thermal fluctuations of the plasma particles [18]. Note that when a strong magnetic field is applied, the behaviors of free electrons and ions in plasmas accounting for the spherical shielding effects would be modified, and as a result, the interparticle interaction of 2D magnetized dusty plasmas could be much more complicated than the Yukawa interaction. Anyway, here we assume that the interparticle interaction is still the Yukawa interaction, as a rough approximation, as in [17].

Yukawa systems are typically characterized by the values of the coupling parameter Γ and the screening parameter κ, where

$$\Gamma = Q^2/(4\pi\epsilon_0 a k_B T)$$

and

$$\kappa \equiv a/\lambda_D,$$

respectively. Here, $a = (\pi n)^{-\frac{1}{2}}$ is the Wigner-Seitz radius [28] and n is the areal number density of particles. In our simulation, we specify the values of κ and Γ as the inputs in simulations. We choose $\kappa = 2.0$. For this value, the melting point of an unmagnetized 2D Yukawa crystal would be $\Gamma = 396$, based on the simulation results in [30].

The perpendicular magnetic field is characterized using the dimensionless parameter $\beta = \omega_c/\omega_{\rm pd}$ as in [16] and [17], where ω_c is the cyclotron frequency of the dust particle, and $\omega_{\rm pd} = (Q^2/2\pi\epsilon_0 m a^3)^{1/2}$ is the nominal dusty plasma frequency [28]. We set the values of β varying from 0 to 1 with a step of 0.1, ranging from 0 to an extremely strong magnetic field as explained in [17]. The frictional gas drag coefficient ν is chosen as $\nu = 0.027\omega_{\rm pd}$, at a level comparable to that in experiments [24]. The simulation box is chosen to be $61.1a \times 52.9a$, and we truncate the Yukawa potential at distances beyond a cutoff radius of $24.8a$, as in [17].

The integration time step for the equation of motion is chosen from the range between $0.0093\omega_{\rm pd}^{-1}$ and $0.037\omega_{\rm pd}^{-1}$, depending on the Γ value [43], as justified in [29]. For all simulation runs, we start from a random configuration of dust particles and use a thermostat in the initial frictionless MD simulation to reach the desired temperature, i.e., the Γ value. Then the Langevin MD simulation is performed in the next 10^7 steps, and the generated data are used for our data analysis reported here. Other simulation details can be found in [17]. Note that, besides the simulation results reported here, we have also performed a few test runs with different initial configurations of particles, and with different numbers of particles from 4096 to 16 384, and our viscosity results were not affected.

B. Green-Kubo relation

In statistical mechanics, there are several Green-Kubo relations to calculate transport coefficients including diffusion, viscosity, and thermal conductivity [44] based on the random thermal motion of particles at equilibrium. The Green-Kubo relation is generally used to calculate the shear viscosity η of frictionless equilibrium systems [29,44], as well as Langevin systems with a modest level of friction as in dusty plasma experiments [45]. Furthermore, the Green-Kubo relation has also been used with experimental data to estimate the viscosity, as in [20] and [42].

In the Green-Kubo relation, the shear viscosity η can be calculated in three steps. First, the off-diagonal element of the shear stress tensor $P_{xy}(t)$ is calculated as

$$P_{xy} = \sum_{i=1}^{N}\left[m v_{ix} v_{iy} - \frac{1}{2}\sum_{j\neq i}^{N}\frac{x_{ij}y_{ij}}{r_{ij}}\frac{\partial\phi(r_{ij})}{\partial r_{ij}}\right], \qquad (1)$$

where N is the total number of particles, m is the mass of one dust particle, and $\phi(r_{ij})$ and $r_{ij} = |\mathbf{r}_i - \mathbf{r}_j|$ are the potential energy and the distance between particle i and particle j, respectively. Then the shear stress autocorrelation function

(SACF) is calculated as

$$C_s(t) = \langle P_{xy}(t) P_{xy}(0) \rangle. \quad (2)$$

Finally, the shear viscosity η can be obtained by integrating the SACF over time using

$$\eta = \frac{1}{VkT} \int_0^\infty C_\eta(t) dt. \quad (3)$$

Here, V is the simulation volume, which should be replaced with the area of the simulation box for 2D systems as reported here. The shear stress, Eq. (1), scales as the system size, while η is independent of the system size.

Although the units for mass density and viscosity are different in two and three dimensions, the units are the same for the kinematic viscosity, which is defined as the ratio of the viscosity to the mass density η/ρ [20,35,38]. For our 2D dusty plasma simulations, the kinematic viscosity can be easily derived as

$$\eta/\rho = \frac{1}{NmkT} \int_0^\infty C_\eta(t) dt. \quad (4)$$

For the calculation method of the shear viscosity above, the required inputs are just the time series of positions, the velocities, and the potential energy ϕ of each particle, which are all available in our Langevin MD simulations.

For two reasons, we describe the result of our Green-Kubo calculations as an estimate of the viscosity, rather than as a precise determination. First, in the experiment in [42], Haralson and Goree found a difference as large as 60% in the values of the viscosity coefficients obtained by the Green-Kubo method compared to the hydrodynamic method. Second, it is still an open question whether transport coefficients for 2D systems really exist, and there have been quite a few discussions about the validity of transport coefficients [20,29,44,46–49]. Some theoretical investigations [46,47] suggest that, for 2D hard disk systems, the autocorrelation function in the Green-Kubo relation decays as slowly as $1/t$, which is called the long-time tail, so that the time integral does not converge. If the transport coefficient does not exist in the Green-Kubo relation, in practice, it means that the measured value of the transport coefficient using another method, like the constitutive equation, would typically depend on the system size, and not be a constant. However, for other 2D systems with different interparticle interactions, some theoretical investigations [20,29,44] have found faster decays in the autocorrelation functions, suggesting that probably transport coefficients are still meaningful for these systems under these conditions. For all data presented below, we have checked that the long-time tail decays more rapidly than $1/t$, over the finite time range available in our simulations.

III. RESULTS

A. Viscosity trend in the cold liquid state

Our results obtained for the SACF and their integrals for the cold 2D liquid dusty plasma ($\Gamma = 200$ and $\kappa = 2.0$) are shown in Fig. 1. In Fig. 1(a), as the external magnetic field increases, the decay of the SACF becomes slower. As a result, the integral of the SACF, as shown in Fig. 1(b), reaches higher levels for larger values of β. As in [20], the upper limit of the integral in Eq. (4) is typically replaced by the time at which C_s first crosses 0 t_I, so that the first maximum point on the integration curve is the obtained viscosity value, as the arrows show in Fig. 1(b). In Fig. 1(b), as the magnetic field increases, the first maximum point gradually increases.

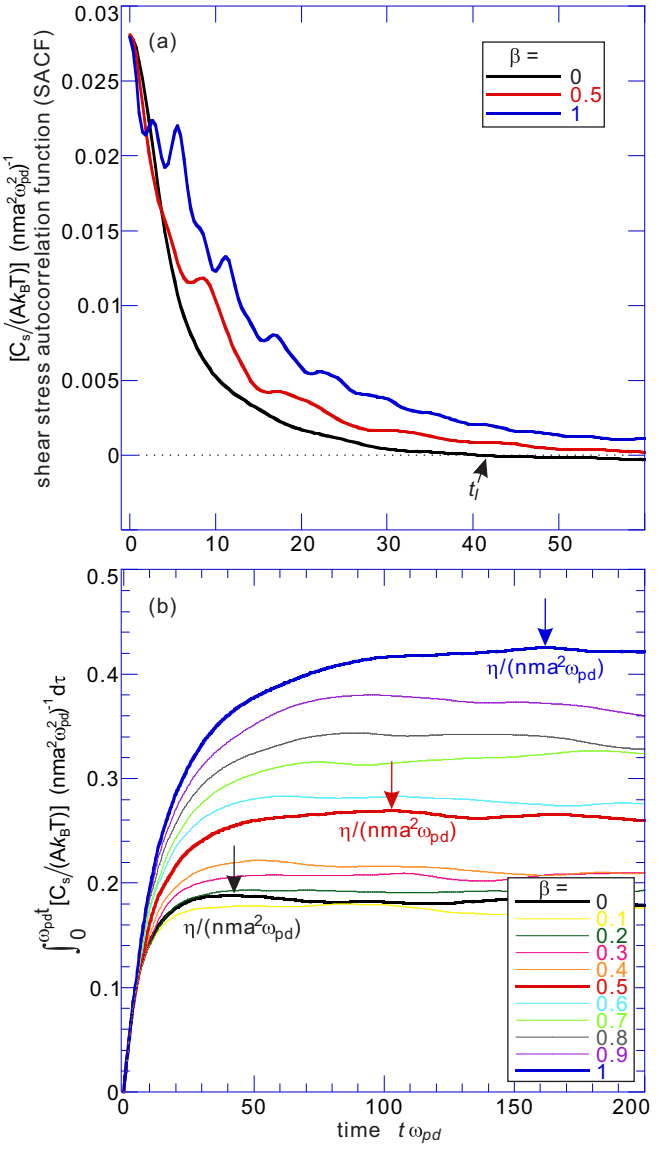

FIG. 1. (a) The shear stress autocorrelation function (SACF) and (b) its time integral for cold 2D liquid dusty plasma with the condition $\Gamma = 200$ and $\kappa = 2$ under different perpendicular magnetic fields. With a higher magnetic field (higher β), the decay of SACF is slower, so that its time integral is larger. From the Green-Kubo relation, the viscosity is obtained as the time integral of the SACF, while the upper limit of the integral is chosen as the first zero point of the SACF [20], labeled t_I. The resulting value of the viscosity is the first maximum of the time integral of the SACF in (b), where three viscosity values are shown by arrows.

In Fig. 1(a), there are ripples in the SACF when β is not 0. These ripples would become stronger when β is larger, suggesting that the ripples are caused by the cyclotron motion due to the external magnetic field. As discovered in [5] and [17], under perpendicular magnetic fields, the thermal motion

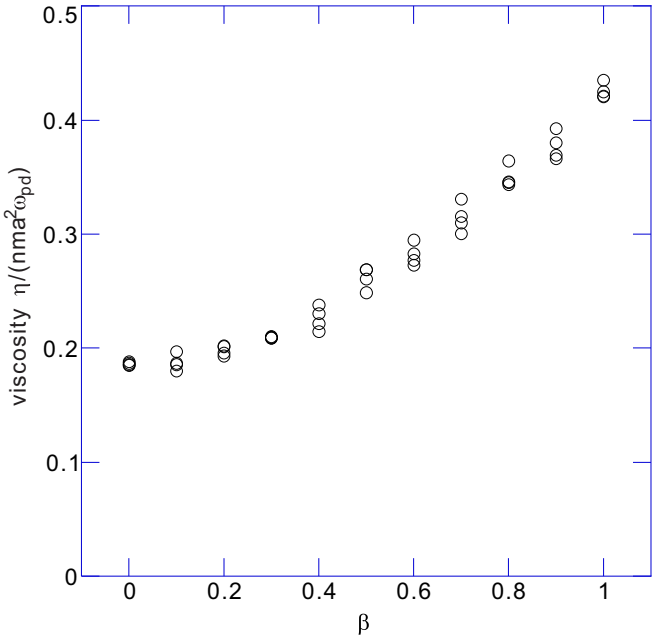

FIG. 2. The shear viscosity of cold 2D liquid dusty plasma with the condition $\Gamma = 200$ and $\kappa = 2$ under different perpendicular magnetic fields. The viscosity of cold 2D liquid dusty plasma, from simulation data using the Green-Kubo method, increases with the magnetic field. For each β value, there are four independent data points obtained from four independent runs, and the scatter of these data would correspond to the error bar.

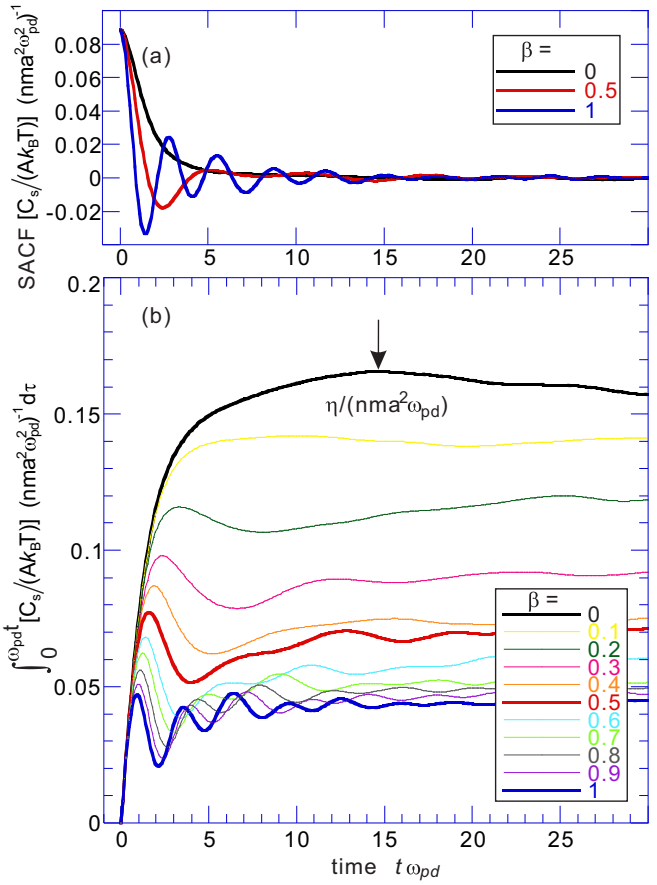

FIG. 3. (a) The SACF and (b) its time integral for hot 2D liquid dusty plasma with the condition $\Gamma = 8$ and $\kappa = 2$ under different perpendicular magnetic fields. With a higher magnetic field or β value, the decay of the SACF is quicker, so that its time integral (viscosity) is smaller.

of 2D dusty plasma has been coupled with the cyclotron motion. In Sec. III C, we investigate the ripples in detail.

In Fig. 2, we present our obtained viscosity values for cold 2D dusty plasma under different magnetic fields using the method above. For each value of β, there are four data points, calculated from four independent simulation runs. We find that, under the dusty plasma condition $\Gamma = 200$ and $\kappa = 2.0$, the shear viscosity generally increases with the external magnetic field. The only exception is at $\beta = 0.1$, where the viscosity is a bit lower than the viscosity at $\beta = 0$ for some data points. From these results, we conclude that, for cold liquid 2D dusty plasmas, the shear viscosity generally increases as the external perpendicular magnetic field increases.

B. Viscosity trends in hot and intermediate liquid states

To test whether the trend observed in Sec. III A is generally valid for other conditions, we simulate hot and intermediate liquid states.

Figure 3 presents the SACF and their integrals for hot liquid dusty plasma under different magnetic fields. For hot liquid dusty plasma, as the magnetic field increases, the SACF decays much more rapidly, as shown in Fig. 3(a), which is completely different from the cold case. In Fig. 3(b), as the magnetic field increases, the final integral of the obtained SACF decreases monotonically. Thus, we can draw the conclusion that, for hot liquid 2D dusty plasmas, the shear viscosity decreases as the magnetic field increases.

The ripples in the SACF are much more severe in Fig. 3 for the hot liquid state than those in Fig. 1 for the cold liquid state. For the cold liquid state in Fig. 1, although there are small ripples, they do not much affect the general decaying trend of the SACF. We are still able to obtain the value of the kinematic viscosity, as in Fig. 2. However, for the hot liquid state, the ripples have such a high amplitude that the general decaying trend of the SACF has been completely modified. The previous choice of the upper limit of the integral in Eq. (4), the time when C_s first crosses 0 t_I, is drastically affected by the individual cyclotron motion. As a result, it is questionable whether t_I can really reflect the decay of the collective behavior of the shear stress. It is ambiguous to determine which maximum point on the integral curve of the SACF would really be related to the viscosity. To avoid this confusion, henceforth, we directly present the SACF integral curve to let readers determine the level of the viscosity and its uncertainty to a degree that is sufficient to assess the trends as the magnetic field is varied.

Figure 4 presents the integrations of the SACF for two intermediate liquid dusty plasmas under various perpendicular magnetic fields. For both conditions in Fig. 4, as the magnetic field increases, the variational trend of the viscosity, or the SACF integration, is no longer monotonic. It seems that, as the dimensionless magnetic field parameter β increases from 0 to 1, the integral of the SACF for long times first decays and then increases gradually after roughly $\beta \geqslant 0.5$.

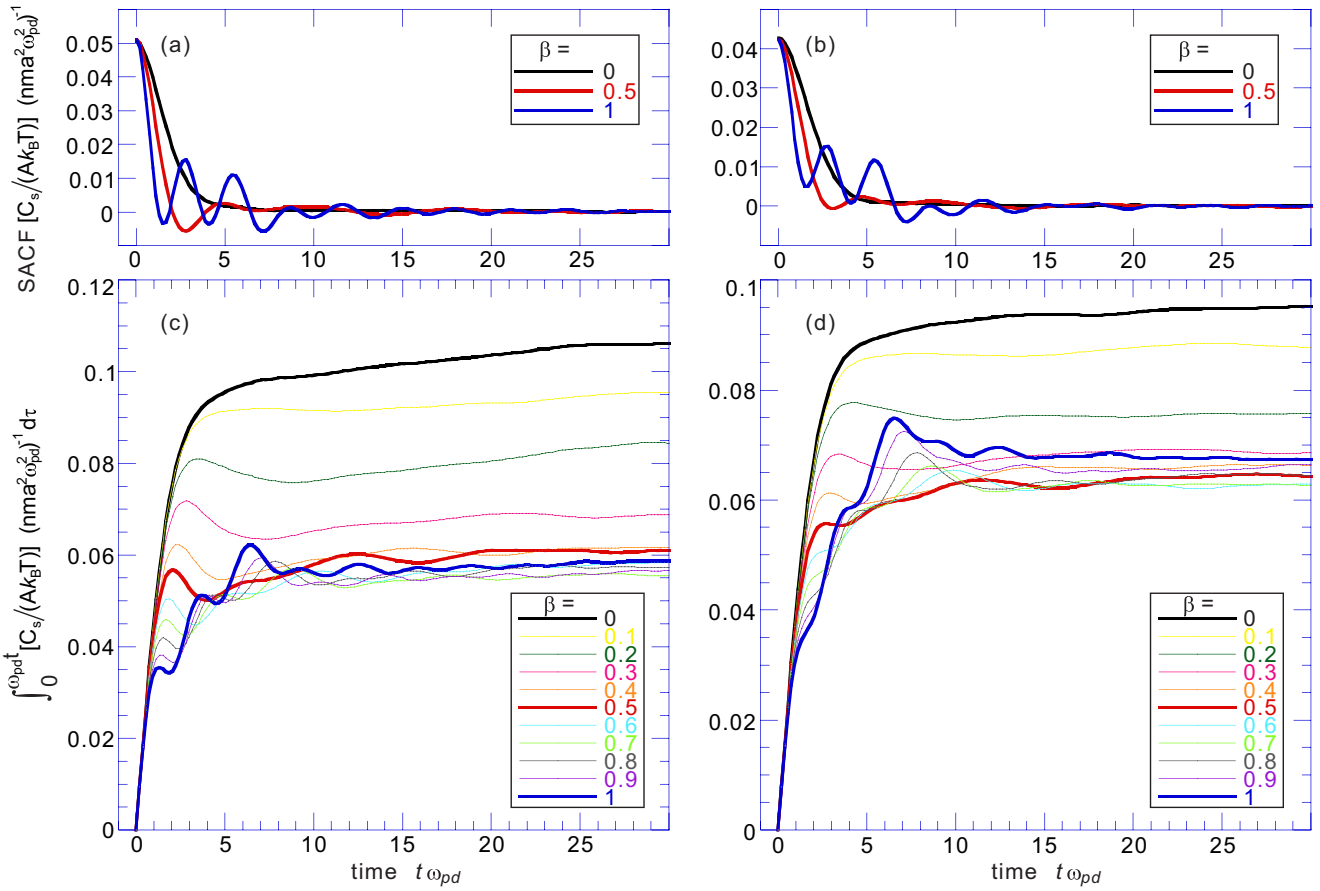

FIG. 4. The SACF and its time integral for 2D liquid dusty plasma at intermediate temperatures, with $\kappa = 2$ while (a, c) $\Gamma = 20$ and (b, d) $\Gamma = 30$, respectively. In (c) and (d), as β increases from 0, the time integral of the SACF decreases substantially at first, and then for β greater than about 0.5, the integral of the SACF increases gradually.

C. Behaviors of various contributions to the viscosity

In our simulation results, we have found opposite trends: for cold 2D liquid dusty plasma, the viscosity increases with the external perpendicular magnetic field, while for hot 2D liquid dusty plasma, it diminishes. In the intermediate temperature range, as the magnetic field increases from 0, its viscosity first diminishes, then increases gradually. To better understand these trends, we split the terms of the shear stress in Eq. (1).

From Eq. (1), the shear stress is composed of two parts: the kinetic part $P_{xy}^{\rm kin}(t) = \sum_{i=1}^{N} m v_{ix} v_{iy}$ and the potential part $P_{xy}^{\rm pot}(t) = -(1/2)\sum_{i=1}^{N}\sum_{j\neq i}^{N}(x_{ij}y_{ij}/r_{ij})(\partial\phi(r_{ij})/\partial r_{ij})$. As a result, the SACF can be expressed as the summation of three terms:

$$\begin{aligned} C_s(t) &= \left\langle P_{xy}^{\rm kin}(t) P_{xy}^{\rm kin}(0)\right\rangle + \left\langle P_{xy}^{\rm pot}(t) P_{xy}^{\rm pot}(0)\right\rangle \\ &\quad + 2\left\langle P_{xy}^{\rm kin}(t) P_{xy}^{\rm pot}(0)\right\rangle \\ &= C_s^{\rm KK}(t) + C_s^{\rm PP}(t) + 2C_s^{\rm KP}(t). \end{aligned} \tag{5}$$

The first term $C_s^{\rm KK}(t)$ and the second term $C_s^{\rm PP}(t)$ are the self-correlation functions of the kinetic and potential parts of the shear stress, respectively. The last term $C_s^{\rm KP}(t)$ is the cross-correlation function between the kinetic and the potential parts.

The three correlation functions of 2D liquid dusty plasmas at different temperatures are presented in Fig. 5. For the cold liquid state, in Figs. 5(j)–5(l), the self-correlation function of the potential part $C_s^{\rm PP}$ is dominant as expected, since the potential part is much larger than the kinetic part in cold liquid states. The situation for the hot liquid state is completely different. As shown in Figs. 5(a)–5(c), the self-correlation function of the kinetic part $C_s^{\rm KK}$ is the largest, since the kinetic part is much larger than that in the cold liquid state. In the intermediate temperature range, $C_s^{\rm KK}$ and $C_s^{\rm PP}$ are roughly comparable, as in Figs. 5(d)–5(i). For all temperature ranges, the cross correlation $C_s^{\rm KP}$ is always the smallest contribution, which is not surprising because the two parts $P_{xy}^{\rm kin}(t)$ and $P_{xy}^{\rm pot}(t)$ are two time series of different physical quantities, which are not much related.

The cyclotron motion of individual particles due to the external magnetic fields can be reflected in ripples of the SACF, $C_s(t)$. Investigating the three contributions of the SACF would lead to more physical insights into these ripples.

For the self-correlation function of the kinetic part $C_s^{\rm KK}$, there are always obvious ripples at different temperatures when $\beta \neq 0$. From Eq. (1), the kinetic part of the shear stress is proportional to the summation of the product of v_{ix} and v_{iy} for all particles. When $\beta \neq 0$, the cyclotron motion causes both v_{ix} and v_{iy} to oscillate, and as a result, the first term

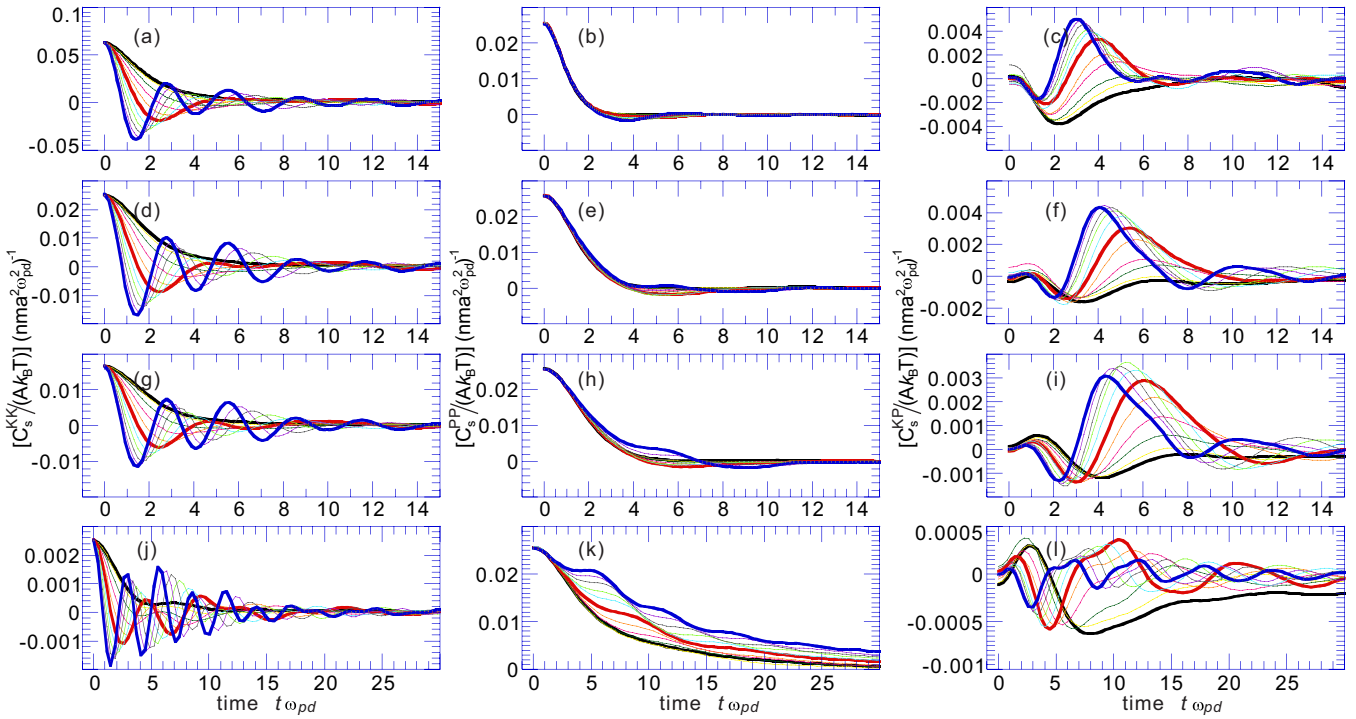

FIG. 5. Three components of the SACF $[C_s^{KK}(t), C_s^{PP}(t), C_s^{KP}(t)]$ for 2D liquid dusty plasma at various temperatures, with $\kappa = 2$ while (a–c) $\Gamma = 8$, (d–f) $\Gamma = 20$, (g–i) $\Gamma = 30$, and (j–l) $\Gamma = 200$, respectively. In the hot 2D liquid dusty plasma, the self-correlation function of the kinetic part C_s^{KK} (a) is dominant in the three components, while in the cold 2D liquid dusty plasma, the self-correlation function of the potential part C_s^{PP} (k) plays a leading role. In the intermediate temperature range, C_s^{KK} and C_s^{PP} have comparable magnitude levels. The cross-correlation C_s^{KP} is always the smallest, for all temperature ranges. Here, the legend for the curves is the same as in Figs. 3 and 4.

in Eq. (1), the product of v_{ix} and v_{iy}, also oscillates, even more quickly. In Fig. 5, the relative magnitude of ripples in C_s^{KK} at low temperatures is smaller than that of ripples at high temperatures. However, in cold liquid states, the decay of C_s^{KK} is slower, and as a result, the ripples' magnitude also appears to be substantial. For hot liquid states, the C_s^{KK} curve decays so quickly that only a few ripples survive.

Compared with C_s^{KK}, the self-correlation function of the potential part of C_s^{PP} shows completely different behavior. For all simulated temperatures, only in the cold liquid state does the C_s^{PP} show clear ripples. In principle, we would expect the lattice of colder liquids to have a longer relaxation time or memory time, and the cyclotron motion would be expected to extend this relaxation (memory) time further. As shown in Fig. 5(k), the decay of the potential part of the shear stress with a larger β is slower, and the ripples caused by the cyclotron motion can be clearly observed. However, at hot and intermediate temperatures, C_s^{PP} decays very quickly, as in Figs. 5(b), 5(e) and (h). When the peak rippling takes place, C_s^{PP} has already decayed to a very low level, and as a result, ripples cannot be easily observed.

D. Conceptual discussion of viscosity variational trends

From the behaviors of the three contributions to C_s studied above, for 2D liquid dusty plasmas, the different variational trends of the viscosity as a function of the external magnetic field can be investigated further. In Fig. 5, with a higher magnetic field, ripples in C_s^{KK} will clearly reduce its integral over time, or the C_s^{KK} contribution to the viscosity. When the magnetic field is smaller, the C_s^{KK} contribution to the viscosity is larger. However, the behavior of C_s^{PP} is completely different. In hot liquid states, the difference in C_s^{PP} is nearly negligible, so that the difference in its contribution to the viscosity is also negligible. In cold liquid states, when the magnetic field is higher, the C_s^{PP} curve decays much more slowly; as a result, its time integration increases dramatically or the C_s^{PP} contribution to the viscosity is larger.

Thus, we can better understand the different variational trends in the viscosity with the external magnetic fields. For the cold liquid state, the viscosity is mainly contributed by the self-correlation of the potential part of the shear stress C_s^{PP}. With external magnetic fields, the decay time of C_s^{PP} increases dramatically, and as a result, its time integral is larger or its viscosity is higher. However, for the hot liquid state, the viscosity is largely dominated by the self-correlation of the kinetic part of the shear stress C_s^{KK}. Under external magnetic fields, the ripples C_s^{KK} would greatly suppress its integral, thus the viscosity is lower with higher magnetic fields. For the intermediate state, these two mechanisms are comparable and competing, so that the variational trend is no longer monotonic.

It is interesting to compare the trends observed above to the conclusion estimated from the Braginskii equations [50]. As series of fluid equations for the electrons and ions in plasmas, the Braginskii equations are more suitable for prediction of the transport behaviors of low-density, high-temperature plasmas [50]. Using the Braginskii equations, the shear viscosity can be estimated, $\eta \propto \nu_c/B^2$, where ν_c is the collision frequency, suggesting that the viscosity diminishes with the magnetic

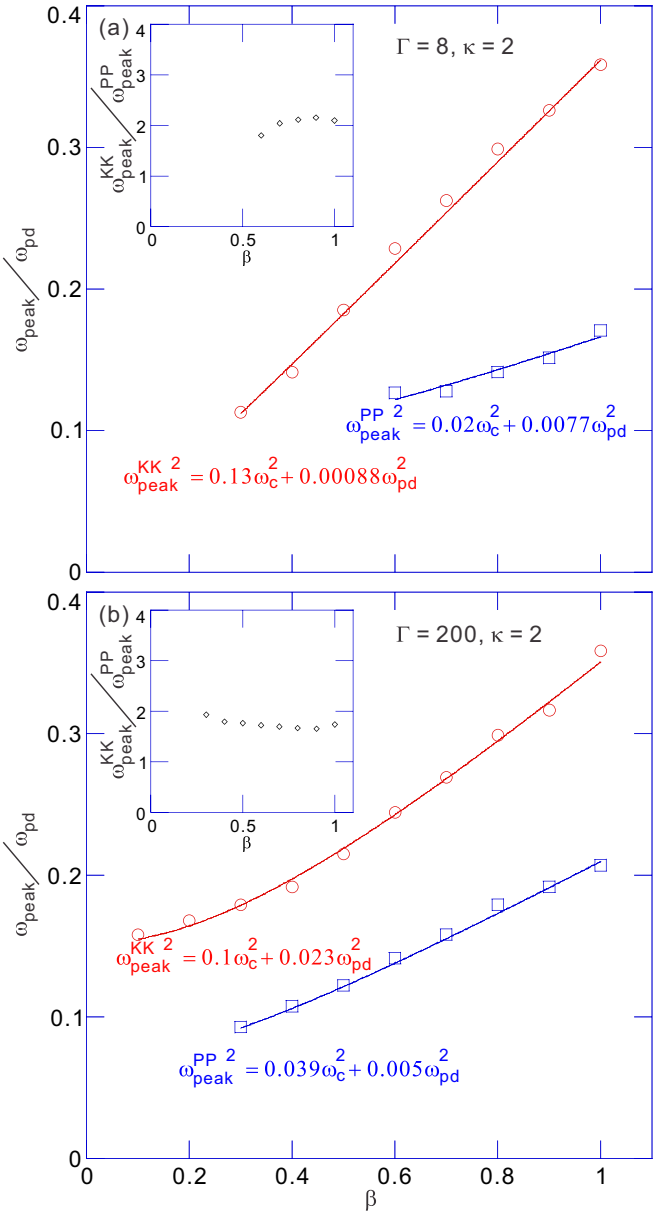

FIG. 6. Frequencies of the ripples in C_s^{KK} and C_s^{PP} for the conditions of (a) $\Gamma = 8$ and (b) $\Gamma = 200$, while $\kappa = 2$. These frequencies are obtained from the times when the first ripple peak occurs in the curves for either C_s^{KK} or C_s^{PP}. From data fitting, we obtain the analytical expressions for these frequencies, which are $\omega_{peak}^{KK\ 2} = 0.13\omega_c^2 + 0.00088\omega_{pd}^2$ and $\omega_{peak}^{PP\ 2} = 0.02\omega_c^2 + 0.0077\omega_{pd}^2$ for $\Gamma = 8$ and $\omega_{peak}^{KK\ 2} = 0.1\omega_c^2 + 0.023\omega_{pd}^2$ and $\omega_{peak}^{PP\ 2} = 0.039\omega_c^2 + 0.005\omega_{pd}^2$ for $\Gamma = 200$. Insets: Illustrations that the ratios of these two frequencies are both close to 2.

field. This predicted trend using the Braginskii equations is exactly the same as our observed trend for high-temperature dusty plasmas, which is more suitable for the Braginskii equations. When the temperature is low, the Braginskii equations are no longer accurate [51,52]; the results from our simulations show an inverse trend of the viscosity increasing with the magnetic field.

E. Time scales of correlation functions

The cyclotron motion caused by the perpendicular magnetic field results in ripples in the SACF, as shown in Figs. 2–4. When the magnetic field is stronger, i.e., the β value is higher, the ripples' amplitude is higher. At all four temperatures studied here, the first ripple peak of the SACF happens at the first ripple peak of C_s^{KK}, and the second ripple peak of the SACF happens at the first ripple peak of C_s^{PP}. The ripples of C_s^{KK} and C_s^{PP} at the four temperatures studied here can be seen in Fig. 5.

We have also quantified the time scales of these ripples for the hot and cold conditions, as shown in Fig. 6. The frequencies of ω_{peak}^{KK} or ω_{peak}^{PP} plotted here are obtained from the times when the first ripple peak occurs in the curves of either C_s^{KK} or C_s^{PP}. For both conditions, as the magnetic field is stronger, their ripple frequencies increase monotonically. We have also obtained analytical expressions using data fitting for these ripple frequencies, as shown in Fig. 6.

One interesting point is that, for all four temperatures studied here, the ripple frequency for C_s^{KK} is always roughly twice the ripple frequency for C_s^{PP}, as shown in the two insets in Fig. 6. We speculate that maybe this roughly doubled frequency for C_s^{KK} is caused by the product of v_x and v_y, which both roughly oscillate with the cyclotron frequency, as demonstrated in Fig. 5(b) in [17].

Note that, in preparing Fig. 6, for some conditions, the first ripple of C_s^{KK} or C_s^{PP} cannot be easily identified if the magnetic field is not large enough; we ignore this data point completely. Also, due to the finite temporal resolution in our MD simulation, the exact time at which the first peak occurs may contain some uncertainties.

IV. SUMMARY

In summary, we have studied the shear viscosity of 2D liquid dusty plasmas under perpendicular magnetic fields using Langevin dynamics simulations. Using the Green-Kubo relation, we have estimated the viscosity, which has been modified substantially with the applied perpendicular magnetic field. We have found that, when the magnetic field is magnified, its viscosity increases at low temperatures, while at high temperatures, its viscosity diminishes. We found that these different variational trends of η are caused by the different behaviors of the kinetic and potential parts of the shear stress under external magnetic fields.

ACKNOWLEDGMENTS

This work was supported by the National Natural Science Foundation of China under Grant No. 11505124, the 1000 Youth Talents Plan, and startup funds from Soochow University. W.L. thanks Maker Space of the Suzhou National New & Hi-Tech Industrial Development Zone for support.

[1] S. Ichimaru, Rev. Mod. Phys. **54**, 1017 (1982).

[2] V. E. Fortov, A. V. Ivlev, S. A. Khrapak, A. G. Khrapak, and G. E. Morfill, Phys. Rep. **421**, 1 (2005).

[3] G. E. Morfill and A. V. Ivlev, Rev. Mod. Phys. **81**, 1353 (2009).
[4] A. Piel, *Plasma Physics* (Springer, Heidelberg, 2010).
[5] M. Bonitz, C. Henning, and D. Block, Rep. Prog. Phys. **73**, 066501 (2010).
[6] R. L. Merlino and J. A. Goree, Phys. Today **57**(7), 32 (2004).
[7] M. J. Jensen, T. Hasegawa, J. J. Bollinger, and D. H. E. Dubin, Phys. Rev. Lett. **94**, 025001 (2005).
[8] J. Castro, P. McQuillen, and T. C. Killian, Phys. Rev. Lett. **105**, 065004 (2010).
[9] J. Hughto, A. S. Schneider, C. J. Horowitz, and D. K. Berry, Phys. Rev. E **82**, 066401 (2010).
[10] C. J. Horowitz, D. K. Berry, and E. F. Brown, Phys. Rev. E **75**, 066101 (2007).
[11] G. Federici, C. H. Skinner, J. N. Brooks, J. P. Coad, C. Grisolia, A. A. Haasz, A. Hassanein, V. Philipps, C. S. Pitcher, J. Roth, W. R. Wampler, and D. G. Whyte, Nucl. Fusion **41**, 1967 (2001).
[12] C. Nurenberg, Phys. Plasmas **3**, 2401 (1996).
[13] J. D. Lindl, P. Amendt, R. L. Berger, S. G. Glendinning, S. H. Glenzer, S. W. Haan, R. L. Kauffman, O. L. Landen, and L. J. Suter, Phys. Plasmas **11**, 339 (2004).
[14] D. D. Ryutov, M. S. Derzon, and M. K. Matzen, Rev. Mod. Phys. **72**, 167 (2000).
[15] C. Kouveliotou, S. Dieters, T. Strohmayer, J. van Paradijs, G. J. Fishman, C. A. Meegan, K. Hurley, J. Kommers, I. Smith, D. Frail, and T. Murakami, Nature **393**, 235 (1998).
[16] T. Ott, H. Löwen, and M. Bonitz, Phys. Rev. E **89**, 013105 (2014).
[17] Y. Feng, J. Goree, B. Liu, T. P. Intrator, and M. S. Murillo, Phys. Rev. E **90**, 013105 (2014).
[18] Y. Feng, J. Goree, and B. Liu, Phys. Rev. Lett. **100**, 205007 (2008); Phys. Rev. E **78**, 026415 (2008).
[19] E. Thomas Jr., J. D. Williams, and J. Sliver, Phys. Plasmas **11**, L37 (2004).
[20] Y. Feng, J. Goree, B. Liu, and E. G. D. Cohen, Phys. Rev. E **84**, 046412 (2011).
[21] H. Yukawa, Proc. Phys.-Math. Soc. Jpn. **17**, 48 (1935).
[22] U. Konopka, G. E. Morfill, and L. Ratke, Phys. Rev. Lett. **84**, 891 (2000).
[23] C.-L. Chan and Lin I, Phys. Rev. Lett. **98**, 105002 (2007).
[24] Y. Feng, J. Goree, and B. Liu, Phys. Rev. Lett. **105**, 025002 (2010).
[25] P. Hartmann, A. Z. Kovács, A. M. Douglass, J. C. Reyes, L. S. Matthews, and T. W. Hyde, Phys. Rev. Lett. **113**, 025002 (2014).
[26] K. Qiao and T. W. Hyde, Phys. Rev. E **68**, 046403 (2003).
[27] Z. Donkó, P. Hartmann, and G. J. Kalman, Phys. Rev. E **69**, 065401(R) (2004).
[28] G. J. Kalman, P. Hartmann, Z. Donkó, and M. Rosenberg, Phys. Rev. Lett. **92**, 065001 (2004).
[29] B. Liu and J. Goree, Phys. Rev. Lett. **94**, 185002 (2005).
[30] P. Hartmann, G. J. Kalman, Z. Donkó, and K. Kutasi, Phys. Rev. E **72**, 026409 (2005).
[31] Z. Donkó, J. Goree, P. Hartmann, and K. Kutasi, Phys. Rev. Lett. **96**, 145003 (2006).
[32] Z. Donkó and P. Hartmann, Mod. Phys. Lett. B **21**, 1357 (2007).
[33] T. Ott, M. Stanley, and M. Bonitz, Phys. Plasmas **18**, 063701 (2011).
[34] A. Shahzad and M. G. He, Phys. Scripta **87**, 035501 (2013).
[35] Y. Feng, J. Goree, and B. Liu, Phys. Rev. E **87**, 013106 (2013).
[36] T. Ott, M. Bonitz, and Z. Donkó, Phys. Rev. E **92**, 063105 (2015).
[37] T. Ott, Z. Donkó, and M. Bonitz, Contrib. Plasma Phys. **56**, 246 (2016).
[38] V. Nosenko and J. Goree, Phys. Rev. Lett. **93**, 155004 (2004).
[39] Y. Feng, J. Goree, and B. Liu, Phys. Rev. Lett. **109**, 185002 (2012).
[40] P. Hartmann, M. C. Sándor, A. Kovács, and Z. Donkó, Phys. Rev. E **84**, 016404 (2011).
[41] Z. Haralson and J. Goree, Phys. Plasmas **23**, 093703 (2016).
[42] Z. Haralson and J. Goree, Phys. Rev. Lett. **118**, 195001 (2017).
[43] Y. Feng, J. Goree, B. Liu, L. Wang, and W. Tian, J. Phys. D: Appl. Phys. **49**, 235203 (2016).
[44] Z. Donkó, J. Goree, P. Hartmann, and B. Liu, Phys. Rev. E **79**, 026401 (2009).
[45] Y. Feng, J. Goree, and B. Liu, Phys. Plasmas **18**, 057301 (2011).
[46] M. H. Ernst, E. H. Hauge, and J. M. J. van Leeuwen, Phys. Rev. Lett. **25**, 1254 (1970).
[47] J. R. Dorfman and E. G. D. Cohen, Phys. Rev. Lett. **25**, 1257 (1970).
[48] T. Ott, M. Bonitz, Z. Donkó, and P. Hartmann, Phys. Rev. E **78**, 026409 (2008).
[49] T. Ott and M. Bonitz, Phys. Rev. Lett. **103**, 195001 (2009).
[50] S. I. Braginskii, in *Reviews of Plasma Physics*, edited by M. A. Leontovich (Consultants Bureau, New York, 1965), Vol. 1, p. 205.
[51] A. B. Mikhailovskii and V. S. Tsypin, Plasmas Phys. **13**, 785 (1971).
[52] P. J. Catto and A. N. Simakov, Phys. Plasmas **11**, 90 (2004).